Preliminary Study of Hyperspectral Unmixing Analysis Associated to Resident Space Objects using DIRSIG™

Aryzbe Najera, Ana C. Chavez-Lopez, Leah Porras, Miguel Velez-Reyes
Electrical and Computer Engineering Department,
The University of Texas at El Paso, 500 W. University Ave., El Paso, USA

ABSTRACT

This paper presents experimental results on hyperspectral unmixing for extracting material composition of resident space objects (RSO) from unresolved imagery (URSO). The study utilizes simulated data generated by a physics-based image simulator, which allow us to have a better understanding and look at changes in the ground-based measured spectral radiance for RSO and URSO satellite to material composition and satellite orientation. The Digital Imaging and Remote Sensing Image Generation (DIRSIG™) simulator is used to simulate ground-based hyperspectral observations of resident space objects. Using a simulation tool allows us to perform controlled computational experiments not possible with observations. The main simulation scene parameters consist of a (1) CAD model for a DirecTV-10 satellite (Boeing 702 Bus); (2) the spectral signatures for the materials assigned to the satellite's surface, (3) the geographic location of the observer (using USAFA-16 Telescope) and satellite via its Two-Line Element (TLE); (4) atmospheric conditions; and (5) the instantaneous field of view (IFOV) determined by the focal length of the optical system. We study the effects of spatial resolution and material composition in the performance of the unmixing process, as well as address the identifiability of materials from the data. We also discuss the resources needed to implement the simulation model in the DIRSIG™ environment.

1. INTRODUCTION

Hyperspectral remote sensing is an approach to extract quantitative information about Resident Space Objects (RSO) to support Space Domain Awareness (SDA). Measured spectral signatures contain information about material composition, pose, spin rate, among other parameters associated to the RSOs. The high spectral resolution provided by hyperspectral imaging allows extracting properties associated to resident space object even if they are not spatially resolved. Consequently, precise spectral signature interpretation may allow us to understand and react appropriately to changing situations in the space domain.

Hyperspectral Unmixing (HU) has been widely used in terrestrial hyperspectral remote sensing to extract sub-pixel material composition information in low to moderate spatial resolution images. The linear mixture model represents this measured signature as a linear combination of the spectral signatures of various materials within the sensor's field of view (FOV). Mathematically,

$$\mathbf{x} = \mathbf{E}\mathbf{a} + \mathbf{w} \tag{1}$$

where $\mathbf{x}$ is the measured spectral signature, $\mathbf{E}$ represents the matrix of the spectral signatures of the materials in the pixel (called endmembers), $\mathbf{w}$ is the vector of noise, and $\mathbf{a}$ is the vector of endmember abundances. Algorithms in terrestrial remote sensing take advantage of spatial domain information to extract endmembers and their abundance from the image. The abundance represents the percentage of each endmember that is present in each pixel of a hyperspectral image [9]. Typically, traditional methods for hyperspectral unmixing involve a three-step approach as follows:

1. Determine the number of endmembers
2. Endmember extraction

3. Abundance estimation

A good review in hyperspectral unmixing can be found in [3]. In this study, we applied two endmember extraction algorithms, (1) a modified version of the Pixel Purity Index (PPI) [4] proposed in [10, 6] and (2) Singular Value Decomposition Subset Selection (SVDSS) [1] to study the effect of image spatial resolution and material composition in the performance of the unmixing pipeline.

2. HYPERSPECTRAL UNMIXING METHODOLOGY

In this section, we present a description for each of the steps involved in the hyperspectral unmixing (HU) workflow.(See Figure 1)

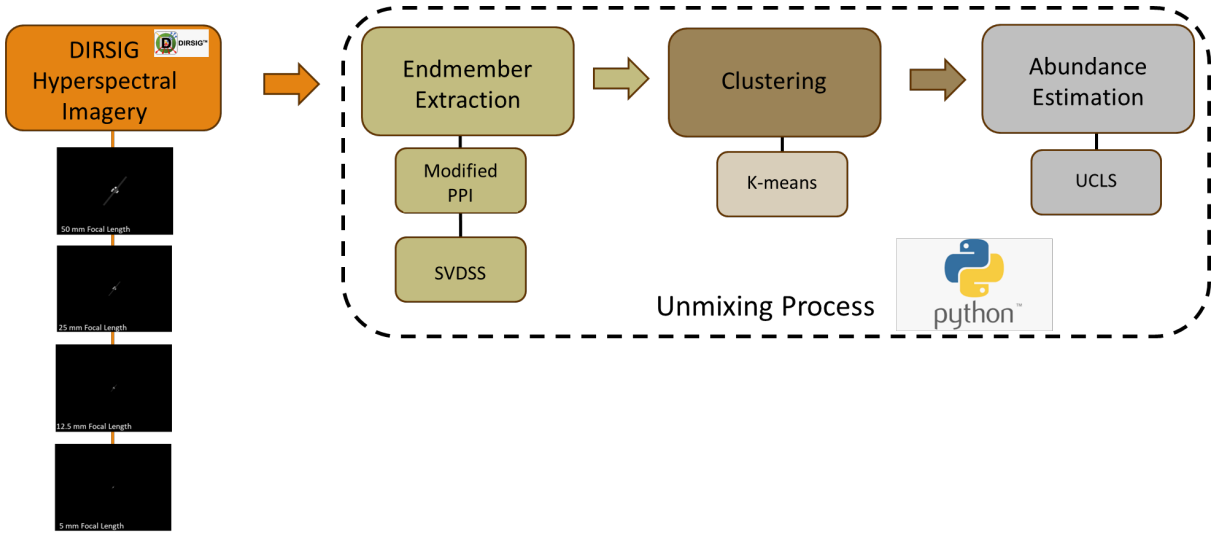

Fig. 1: Hyperspectral Unmixing Workflow.

2.1 HYPERSPECTRAL IMAGERY

We utilize synthetic resolved and unresolved imagery of a satellite based on the CAD model for DirecTV-10 generated by The Digital Imaging and Remote Sensing Image Generation (DIRSIG™) model. This model is developed by Rochester Institute of Technology (RIT) Digital Imaging and Remote Sensing Laboratory [8]. DIRSIG™has the capability to produce passive multidimensional optical imagery (single-band, multi-spectral, polarimetric, or hyperspectral) and simulates images of a wide variety of resolved and non-resolved space objects across from the visible through the thermal infrared region of the electromagnetic spectrum. Additionally, DIRSIG™has been used to simulate time-varying ground and space-based observations of both LEO and GEO objects [2]. In this study, an imaging focal plane array of 320×240 with a pixel width of 0.5μm $\times$ 0.5μm was simulated. Hyperspectral observations were simulated in the 400 nm-2500 nm spectral range with 1 nm spectral resolution. The instantaneous field of view (IFOV), which is the angular resolution, is determined by the ratio of the pixel width to the Focal Length (FL) of the optical system. Additionally, we study the effects of angular resolution in the unmixing process by setting the FL to 50 mm, 25 mm, 12.5 mm, and 5 mm. (See Table 1) Four regions of interest (ROI) were identified from the resolved image (50 mm FL) as follows: (1) background, (2) Solar Panels (Silicon), (3) Bus (Kapton HN), and (4) antennas (Aluminum). (See Figure 2(a)) DIRSIG images at four different focal lengths are shown in Figure 2. The reference endmember spectral signatures associated to the 3 ROIs in the dataset are shown in Figure 3.

3. ENDMEMBER EXTRACTION ALGORITHMS

3.1 Modified Pixel Purity Index (MPPI)

The first endmember extraction algorithm used in this study is a modified version of the Pixel Purity Index (ModPPI). In the traditional PPI [4], spectral vectors are projected onto randomly generated skewers, identifying the maximum

Table 1: DIRSIG™Imagery Characteristics

Characteristics	**DIRSIG™Imagery**
Type of Image	Hyperspectral Image
Detector size	320 X 240 Pixels
Pixel Width	0.5*um* X 0.5*um*
Spectral resolution	1 nm
Simulated Focal Lengths (FL)	50 mm, 25 mm, 12.5 mm, 5 mm
IFOV (angular resolution)	0.1 *um*, 0.05 *um*, 0.025 *um*, 0.01 *um*
Image size	320 lines, 240 samples, 421 bands
Wavelength range	400 - 2500 nm

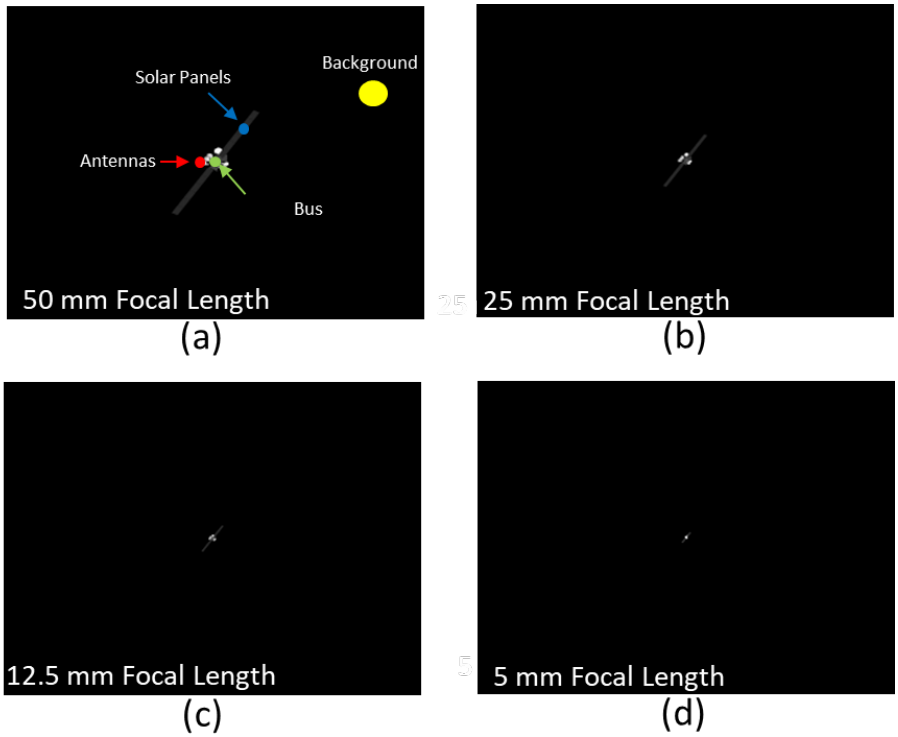

Fig. 2: Simulated Images: (a) 50 mm Focal Length, (b) 25 mm Focal Length, (c) 12.5 mm Focal Length, and (d) 5 mm Focal Length.

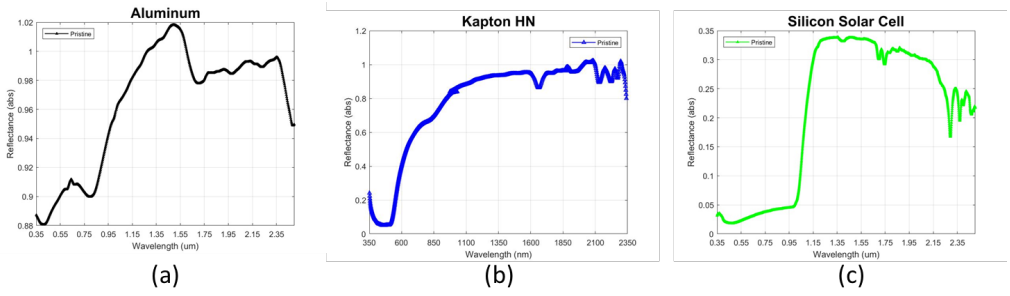

Fig. 3: Endmember spectral signatures: (a) Aluminum, (b) Kapton HN, (c) Silicon Solar Cell. Material signatures were provided by NASA and RIT.

point for each projection. It then tracks how many times a pixel appears as a maximum, selecting the highest-scoring pixels as the purest endmembers. It assumes that the number of endmembers is known. Pixels that appear as maximums most often are considered the purest, or most representative, endmembers in the image. In MPPI, we count the number of times that the pixel appears as a maximum or a minimum in the projection and do not assume that the number of endmembers is known. The number of endmember is selected as the number of pixel that receive the highest number of votes according to a selected threshold. The threshold is selected as all the pixels in the top X% of the projection counts. In this work, the threshold was selected based on trial and error. Future work will explore more systematic approaches. For this study, 4 regions of interest (ROIs) in the image are present (background, satellite panels, payload and antennas). Since some of the selected signatures may be similar, we cluster them using k-means with cosine similarity.

3.2 SVD Column Subset Selection (SVDSS)

SVDSS is an approach to solve the Column Subset Selection Problem (CSSP). CSSP is a problem widely studied in linear algebra and data analytics [5]. A variant of CSSP is one that tries to identify the most independent subset of columns of a matrix $\mathbf{X}$. This problem can be stated as the problem of finding a permutation matrix Π such as:

$$\mathbf{X}\Pi = [\mathbf{X}_1 \mid \mathbf{X}_2] \tag{2}$$

where, $\mathbf{X}_1$ contains the most linearly independent columns of $\mathbf{X}$. This is a combinatorial optimization problem [11], and many algorithms to compute and approximate solution are proposed in the literature [5].

An SVD-based approach to compute a solution to the CSSP in (2) is proposed in [7]. We will denote this approach by SVDSS. The use of SVDSS for endmember extraction was proposed in [1, 12].

Let $\mathbf{X}$ be a matrix representation of the hyperspectral cube that is obtained by unfolding the cube in a way that the columns of $\mathbf{X}$ are the spectral signatures of the pixels in the hyperspectral image and the rows are the bands. Let p be the number of endmembers. In SVDSS, we take the first p right singular vectors for $\mathbf{X}$, $\mathbf{V}_p$ and compute the following QR factorization with pivoting

$$\mathbf{QR} = \mathbf{V}_p^T \Pi \tag{3}$$

The pivoting matrix Π in (3) is the one needed for (2). The reader is referred to [1, 12] for more details.

4. ABUNDANCE ESTIMATION

Once endmember extraction (EE) is completed, the next step in hyperspectral unmixing is to estimate their abundances. This is done by computing $\mathbf{a}$ in (1) solving the constrained linear least squares problem:

$$\widehat{a} = argmin \parallel \mathbf{x} - \mathbf{E}\mathbf{a} \parallel_2^2 \tag{4}$$

where the abundance vector needs to satisfy $\mathbf{a}^T\mathbf{1} = 1$ and $\mathbf{a} \geq 0$. This is known in the unmixing literature as fully constrained abundance estimation problem. In our initial study because we are working with noise free simulated data, we will solve (4) as an unconstrained least squares (UCLS) problem which has as solution

$$\widehat{\mathbf{a}}_{(UCLS)} = (\mathbf{E}^\mathbf{T}\mathbf{E})^{-1}\mathbf{E}^T\mathbf{x} \tag{5}$$

5. EXPERIMENTAL RESULTS

5.1 Modified PPI Results

As mentioned earlier, the Modified PPI (ModPPI) is based on the PPI, where we count the number of times (votes) a pixel appears as a maximum or a minimum in the projection, and the number of endmembers is selected by choosing the spectral signatures in the top X% of received votes. In this experiment, we did 10,000 projections and chose as spectral endmembers the pixels that were in the top 3% of the pixels who received votes. This threshold was selected based on trial and error, and further work is needed for a more systematic approach.

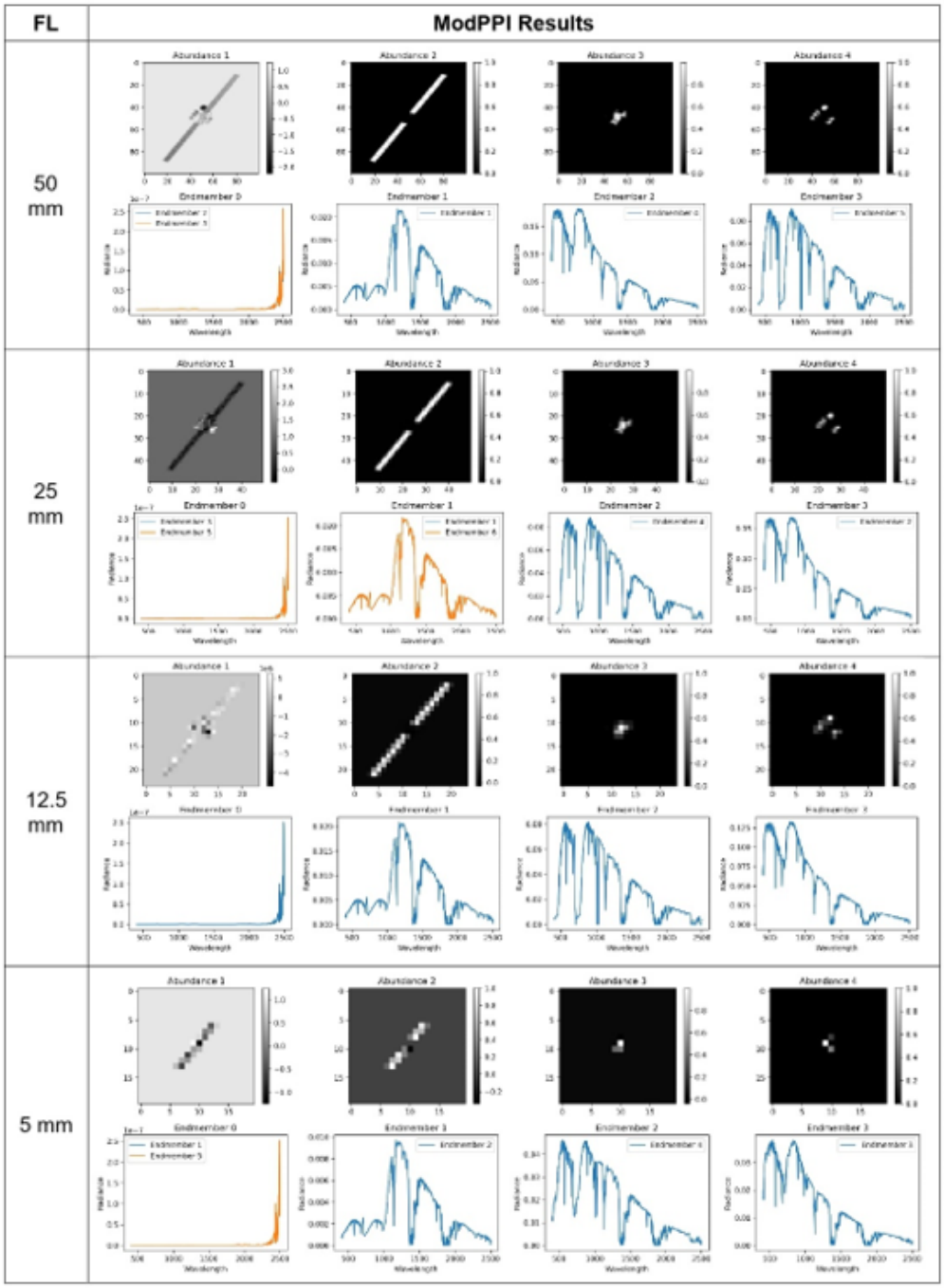

Fig. 4: Endmember signatures and abundances extracted from Modified PPI algorithm

We did the experiment with fully resolved, moderately resolved, and unresolved imagery. We simulated this effect by changing the focal length (FL) of the telescope from 50mm to 5mm while keeping the focal plane detector size constant. In this case, the instantaneous field of view (IFOV) or angular resolution is inversely proportional to the focal length.

For a focal length of 25mm, ModPPI extracted 5 endmembers and for 25mm and 12.5mm, 5 and 14 endmembers respectively. (See Figure 4) In the last case, with a focal length of 5mm, 5 endmembers were extracted. Because some spectral signatures from different pixels were identical, clustering was used to group similar spectral signatures. We call these endmember clusters, endmember classes and individual spectral signatures call them spectral endmembers. For this example, the spectral endmembers were clustered in 4 endmember classes. To get the abundance for each endmember class, we summed up the abundances for each individual spectral endmember. The abundances for all endmembers were computed using (5).

5.2 SVDSS Results

The next algorithm studied in this work was the SVDSS. To used this approach we need to provide the number of endmembers a priori. The experiment was conducted to find 4 endmembers for each focal length. The results shown in Figure 5 demonstrate that the 4 endmembers found correspond to each satellite component for the 50mm FL, 25mm FL, and 12.5mm FL as shown by the abundance maps.

5.3 Discussion

It is important to point out that both methods found the radiance signatures for the different satellite components (panels, Bus and antennas). We used the endmembers from the resolved image at a FL of 50mm as the ”true” spectral radiance signatures. Note that as the FL decreases (IFOV increases) the endmembers that we obtain are not ”pure” but a mixture of the material and other elements. However, the shape of background and solar panels remained quite similar across different focal lengths while the endmembers related to the bus and antennas became mixed. The solar panels were the largest components of the satellite, so this result is not surprising.

Table 2: Linear Regression Results

Focal Length (FL)	Mixed Endmembers	Coeff-1 (Antennas)	Coeff-2 (Bus)	Coeff-3 (Panels)	Coeff-4 (Background)
12.5 mm	Antenna	0.7274	0	0.0066	-2.2272
12.5 mm	Payload Bus	0	0.8944	0.041	0.0157
12.5 mm	Solar Panels	0	0	0.9601	1.1141
5 mm	Antenna	0.1871	0.0512	0	0.4075
5 mm	Payload Bus	0.0999	0.299	0.3489	0.1186
5 mm	Solar Panels	0	0	0.4450	0.7495

To study the relation between pure and mixed endmembers, the least squares linear regression was computed to find the relationship between the ”true” radiance signatures at 50mm against the mixed endmembers at the smaller focal lengths of 12.5mm and 5mm.(See Table 2) Note that the radiance signatures at 50mm and 25mm are almost identical. Note that there are some changes in scale due to the changes in the sensor IFOV. At 12.5 mm we can see how that the antennas and payload bus endmembers are slightly mixed with the solar panels and the background. At 5mm, the antennas endmember is highly mixed with the payload bus and background endmembers while the payload bus is highly mixed with antennas, solar panels, and background endmembers. Note that in both cases the solar panel endmember is only mixed with the background. This is not surprising as this is the largest component of the satellite. Also, the background radiance signature has a much smaller radiance value compared to the other signatures.

6. CONCLUSIONS

In this paper, we studied the unmixing of simulated hyperspectral images of a DirecTV-10 like satellite. We study the effects on the performance of the endmember extraction process as a function of the telescope angular resolution (IFOV). We observed that for the simulated images, we were able to extract signatures associated with the satellite components but as the angular resolution decreased we started to extract mixed endmembers. We also studied two

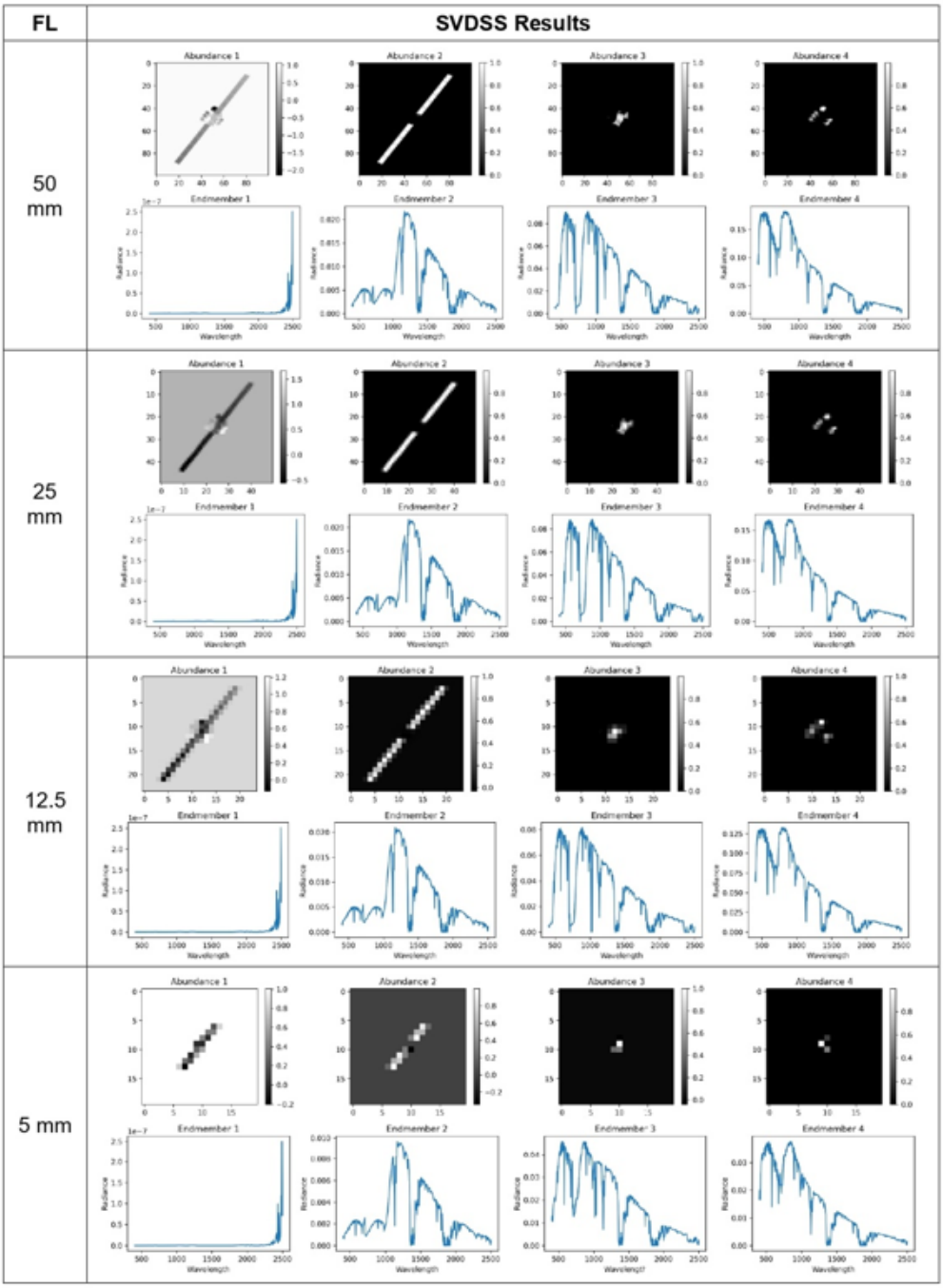

Fig. 5: Endmember signatures and abundances extracted from SVDSS algorithm

endmember extraction algorithms, SVDSS and ModPPI. The unmixing results using PPI and SVDSS are quite consistent and related to the fact that we used simulated noise free imagery. We expect more differences with more realistic simulated data.

SVDSS was the best in extracting the four endmembers present in the simulated data but requires prior knowledge of the number of endmembers. However, ModPPI was capable of extracting all component signatures, and it was able to determine the number of endmember from the data. Work is still needed on an approach to select the threshold to determine the number of endmembers in ModPPI.

7. ACKNOWLEDGEMENTS

This material is based on research sponsored by Air Force Research Laboratory (AFRL) under agreement number FA9453-21-2-0064. The U.S. Government is authorized to reproduce and distribute reprints for Governmental purposes notwithstanding any copyright notation thereon. The views and conclusions contained herein are those of the authors and should not be interpreted as necessarily representing the official policies or endorsements , either expressed or implied, of Air Force Research Laboratory (AFRL) and or the U.S. Government.

8. REFERENCES

[1] Maher Aldeghlawi, Mohammed Q Alkhatib, and Miguel Velez-Reyes. Evaluating column subset selection methods for endmember extraction in hyperspectral unmixing. In *Proceedings of SPIE: Algorithms, Technologies, and Applications for Multispectral and Hyperspectral Imagery XXVI*, volume 11392, pages 275–285. SPIE, 2020.

[2] David A Bennett, Jeff A Dank, David W Tyler, Michael Gartley, and David Allen. Ssa modeling and simulation with dirsig. In *Proceedings of the Advanced Maui Optical and Space Surveillance Technologies Conference, Maui, HI, USA*, pages 9–12, 2014.

[3] José M Bioucas-Dias, Antonio Plaza, Nicolas Dobigeon, Mario Parente, Qian Du, Paul Gader, and Jocelyn Chanussot. Hyperspectral unmixing overview: Geometrical, statistical, and sparse regression-based approaches. *IEEE journal of selected topics in applied earth observations and remote sensing*, 5(2):354–379, 2012.

[4] Joseph W Boardman, Fred A Kruse, and Robert O Green. Mapping target signatures via partial unmixing of aviris data. In *Summaries of the fifth annual JPL airborne earth science workshop. Volume 1: AVIRIS workshop*, 1995.

[5] Mary E Broadbent, Martin Brown, Kevin Penner, Ilse Ipsen, and Rizwana Rehman. Subset selection algorithms: Randomized vs. deterministic. *SIAM undergraduate research online*, 3(01), 2010.

[6] Ana C Chavez-Lopez and Miguel Velez-Reyes. Unmixing analysis of close-range hyperspectral images. In *IGARSS 2023-2023 IEEE International Geoscience and Remote Sensing Symposium*, pages 7543–7546. IEEE, 2023.

[7] Gene Golub, Virginia C Klema, and Gilbert W Stewart. *Rank degeneracy and least squares problems*. Stanford University, 1976.

[8] Adam A Goodenough and Scott D Brown. DIRSIG 5: core design and implementation. In *Proceedings of SPIE: Algorithms and Technologies for Multispectral, Hyperspectral, and Ultraspectral Imagery XVIII*, volume 8390, pages 124–132. SPIE, 2012.

[9] Nathalie Gorretta and Cécile Gomez. *Spectral–Spatial Unmixing Approaches in Hyperspectral VNIR/SWIR Imaging*, volume 30. Elsevier, 2016.

[10] Ana C Chavez Lopez, Manuel M Goez Mora, Maria C Torres-Madroñero, and Miguel Velez-Reyes. Using hyperspectral unmixing for the analysis of very high spatial resolution hyperspectral imagery. In *Proceedings of SPIE: Algorithms, Technologies, and Applications for Multispectral and Hyperspectral Imaging XXIX*, volume 12519, pages 277–284. SPIE, 2023.

[11] Yaroslav Shitov. Column subset selection is np-complete. *Linear Algebra and its Applications*, 610:52–58, 2021.

[12] Miguel Velez-Reyes and Maher Aldeghlawi. Using a column subset selection method for endmember extraction in hyperspectral unmixing. In *Proceedings of SPIE: Algorithms and Technologies for Multispectral, Hyperspectral, and Ultraspectral Imagery XXIV*, volume 10644, pages 83–89. SPIE, 2018.